Electronic structure of dense Pb overlayers on Si(111) investigated using angle-resolved photoemission

W. H. Choi,[1,2] H. Koh,[1,3] E. Rotenberg,[3] and H. W. Yeom[1,2,*]
[1]*Center for Atomic Wires and Layers, Yonsei University, Seoul 120-749, Korea*
[2]*Institute of Physics and Applied Physics, Yonsei University, Seoul 120-749, Korea*
[3]*Advanced Light Source, Lawrence Berkeley National Laboratory, Berkeley, California 94720, USA*
(Received 6 November 2006; revised manuscript received 22 December 2006; published 26 February 2007)

Dense Pb overlayers on Si(111) are important as the wetting layer for anomalous Pb island growth as well as for their own complex "devil's-staircase" phases. The electronic structures of dense Pb overlayers on Si(111) were investigated in detail by angle-resolved photoemission. Among the series of ordered phases found recently above one monolayer, the low-coverage $\sqrt{7}\times\sqrt{3}$ and the high-coverage $14\times\sqrt{3}$ phases are studied; they are well ordered and form reproducibly in large areas. The band dispersions and Fermi surfaces of the two-dimensional (2D) electronic states of these overlayers are mapped out. A number of metallic surface-state bands are identified for both phases with complex Fermi contours. The basic features of the observed Fermi contours can be explained by overlapping 2D free-electron-like Fermi circles. This analysis reveals that the 2D electrons near the Fermi level of the $\sqrt{7}\times\sqrt{3}$ and $14\times\sqrt{3}$ phases are mainly governed by strong 1×1 and $\sqrt{3}\times\sqrt{3}$ potentials, respectively. The origins of the 2D electronic states and their apparent Fermi surface shapes are discussed based on recent structure models.

DOI: 10.1103/PhysRevB.75.075329 PACS number(s): 73.20.−r, 71.18.+y, 79.60.−i

I. INTRODUCTION

Metal overlayers on semiconductor surfaces have been studied extensively for several decades due to both their technological importance and fundamental interest. When group-III, -IV, and -V elements such as indium, lead, and bismuth are deposited on a silicon surface, the solubility of the metallic elements is low enough to form abrupt interfaces.[1] Traditionally, these "ideal interfaces" have played the role of model systems to understand the fundamental aspects of metal-semiconductor interfacial systems such as Schottky barrier formation.[2–6]

Recently, Pb ultrathin films on Si(111) have attracted renewed interest due to the extraordinary manifestation of quantum properties in the unusual growth mode that prefers specific island heights,[7–9] the so-called electronic growth,[10,11] and the clear observation of electron quantization[12] and its consequence for various physical properties such as superconductivity.[13] For most of these fascinating phenomena, the wetting layer, which is thought to consist of about 1.3 monolayer[9] (ML) of Pb on roughly bulk-terminated Si(111), would play an important role in governing the electron scattering at the interface.[14,15] Moreover, the dense Pb wetting layer itself was recently shown to exhibit a complex and intriguing structural property, for which the underlying physics is not fully understood.[16]

At about 1 ML, the Pb overlayer forms a 1×1 phase at room temperature (RT),[17–19] while at a lower coverage the only ordered phase is the well-known $\sqrt{3}\times\sqrt{3}$ phase (nominally at 0.33 ML). The $\sqrt{3}\times\sqrt{3}$ phase has one Pb adatom among three neighboring *T*4 sites of the bulk-terminated Si(111)1×1 layer, saturating all Si dangling bonds as shown in Fig. 1(a).[21] On the other hand, the structure of the 1×1 phase itself is not sufficiently clear. At low temperature, the 1×1 phase is known to undergo a phase transition into a $\sqrt{7}\times\sqrt{3}$ phase.[18–20] The origin of this transition is not known yet and there are controversial structural models for the $\sqrt{7}\times\sqrt{3}$ phase with different Pb coverages of 1.0 [Fig. 1(c)] (Ref. 19) or 1.2 ML [Fig. 1(d)].[21] At slightly higher Pb coverages, various intriguing phases were observed, which have been interpreted as incommensurate phases with hexagonal or striped domain walls.[22,23] However, a more recent study[16] suggested that these complex phases have, in fact, large commensurate unit cells. Furthermore, the competition of two structural units with different densities, the $\sqrt{7}\times\sqrt{3}$ structure of 1.2 ML [Fig. 1(d)] and the dense $\sqrt{3}\times\sqrt{3}$ structure of 1.33 ML [Fig. 1(b)], was suggested to be responsible for the complicated phase diagram, which is a realization of a theoretical model,[24] the "devil's staircase." In that model, a set of numerous commensurate phases with large unit cells can be constructed by the linear combination of two basic building

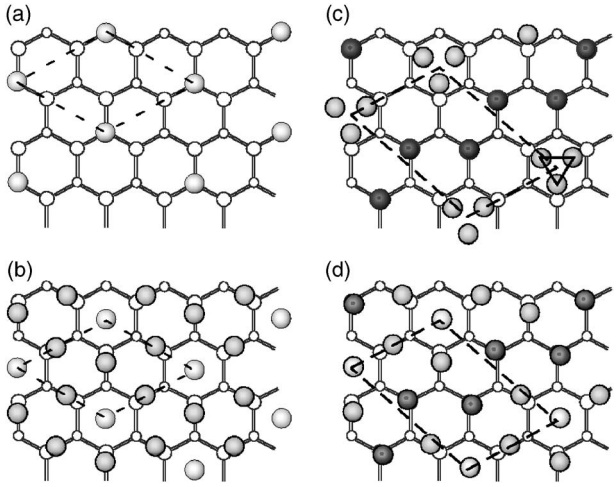

FIG. 1. Schematics of structure models for representative Pb/Si(111) phases: (a) the $\sqrt{3}\times\sqrt{3}$ phase at 0.33 ML of Pb (Ref. 21), (b) $\sqrt{3}\times\sqrt{3}$ at 1.33 ML (Refs. 16 and 21), (c) $\sqrt{7}\times\sqrt{3}$ at 1.0 ML (Ref. 19), and (d) $\sqrt{7}\times\sqrt{3}$ (Ref. 21) at 1.2 ML. Large (small) open circles denote the first- (second-) layer Si atoms and filled circles with different contrasts Pb atoms in different registries.

blocks. However, the devil's-staircase mechanism itself and the structure models of the $\sqrt{7}\times\sqrt{3}$ and the dense-$\sqrt{3}\times\sqrt{3}$ phases remain to be confirmed.

Although closely related to the structural issues mentioned above, the electronic structures of the dense Pb overlayers are largely unknown, with only very early photoemission studies.[6,25] A detailed electronic structure study would be important not only for unraveling the structural issues but also for understanding the microscopic mechanism of the unusual growth mode and the interfacial electron scattering for electron confinement.[8,26] Moreover, the dense Pb overlayers are expected to be strongly metallic and are, therefore, promising candidates for the observation of novel low-dimensional metallic properties.[27] In particular, the devil's-staircase phases would provide a unique set of overlayer phases to study the effect of subtle long-period structural modulations, with only marginal density variation, on two-dimensional (2D) metallic band structures.

In this work, we have investigated the electronic band structures by angle-resolved photoemission (ARP) of two well-ordered dense Pb overlayers on Si(111) with proximal coverages but with distinctly different periodicities and symmetries: the $\sqrt{7}\times\sqrt{3}$ and $14\times\sqrt{3}$ phases. These phases have the lowest and the highest[28] Pb coverages, respectively, among the observed superstructures, representing roughly the two basic building blocks for the devil's-staircase phases. The detailed Fermi surfaces (FS's) are mapped out and the underlying band dispersions are identified. In order to understand the measured FS's, we analyze them based on 2D nearly-free-electron models. As a result, the basic free-electron-like circular Fermi contours are revealed for both surfaces. The apparent overall periodicities of the FS's are characteristically different for the two phases and much simpler than those of the corresponding electron-diffraction patterns: 1×1 for $\sqrt{7}\times\sqrt{3}$ and $\sqrt{3}\times\sqrt{3}$ for $14\times\sqrt{3}$. Such simple and basic features of the FS's and more details of the band structures are discussed in terms of the competing potentials of different periodicities and the atomic structure models.

II. EXPERIMENT

A slightly vicinal Si(111) wafer, miscut by 2° toward $[11\bar{2}]$, was used as a substrate, in order to possibly avoid the formation of multiple domains with different orientations, which make ambiguous the interpretation of spectral features in ARP. The Si wafer was repeatedly flash heated up to 1470 K to get a clean surface and then postannealed at 1123 K carefully to get a regular array of steps and terraces with a well-ordered 7×7 reconstruction.[29] The sample was heated resistively and cooled cryogenically down below 100 K.

After the cleaning process, Pb of slightly more than 2 ML was deposited on the substrate held at RT using an effusion cell. By a subsequent annealing at 550 K, the excess Pb adsorbates were removed and a well-ordered single-domain $14\times\sqrt{3}$ phase was obtained as shown by the low-energy-electron diffraction (LEED) pattern of Fig. 2(a) [its schematics are in Fig. 2(b)]. All LEED patterns were taken below

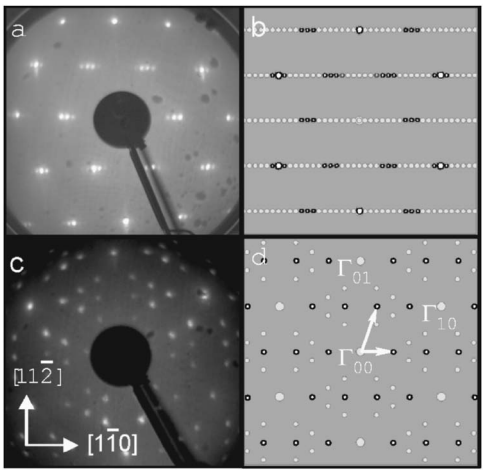

FIG. 2. (a) Low-energy-electron diffraction (LEED) pattern at 122 eV and (b) reciprocal lattice points of the single-domain $14\times\sqrt{3}$ phase. The black circles denote the visible spots in (a). (c) LEED pattern at 88 eV and (d) reciprocal lattice points of the triple-domain $\sqrt{7}\times\sqrt{3}$ phase. The black circles represent the points for a single domain (Ref. 22).

100 K. The black circles in Fig. 2(b) correspond to the visible LEED spots in Fig. 2(a), which are basically the multiple splitoffs of each $\sqrt{3}\times\sqrt{3}$ spot. The overall characteristics of the LEED pattern and the detailed intensity variation of each spot are very similar to those of the $13\times\sqrt{3}$ phase reported recently.[30] In the present case, a "$\times14$" periodicity along the $[1\bar{1}0]$ direction, which is estimated from the average spacing 0.11 Å^{-1} between the adjacent spots, is apparent as shown in Fig. 2(b). In the devil's-staircase phase diagram,[16] the $14\times\sqrt{3}$ phase consists of six dense $\sqrt{3}\times\sqrt{3}$ and two $\sqrt{7}\times\sqrt{3}$ units with a Pb coverage of 1.28 ML, while the $13\times\sqrt{3}$ phase has seven dense $\sqrt{3}\times\sqrt{3}$ and one $\sqrt{7}\times\sqrt{3}$ unit at a slightly higher coverage.

Within the phase diagram, there are many other phases with Pb coverages higher than $14\times\sqrt{3}$ including the highest-coverage (1.33 ML) phase of the dense $\sqrt{3}\times\sqrt{3}$ phase. However, we could not get any such phases with clear and reproducible LEED patterns. That is, the $14\times\sqrt{3}$ phase was, in our own preparation scheme, practically the highest-coverage one within the phase diagram with a reproducible and sufficient long-range order. However, a few other phases with slightly smaller coverages could be obtained by further annealing at a higher temperature and for a longer time. In particular, the lowest-coverage phase of the phase diagram, the $\sqrt{7}\times\sqrt{3}$ phase, was observed in triple domains rotated by 120° as shown in Figs. 2(c) and 2(d). There are six superstructure spots within each triangle made by three neighboring fundamental spots (for example, $\bar{\Gamma}_{00}$, $\bar{\Gamma}_{10}$, and $\bar{\Gamma}_{01}$) of the Si(111)1×1 reciprocal lattice. Among them, only two spots [black circles in Fig. 2(d)] originate from a single domain. Even though we started from a high-coverage single-domain $14\times\sqrt{3}$ phase, the triple-domain formation was inevitable for $\sqrt{7}\times\sqrt{3}$. This indicates that the effect of steps in the lateral growth of these two phases is distinct.

The ARP measurements were performed using intense synchrotron radiation from the soft x-ray undulator beamline

7.0.1.2 at the Advanced Light Source of Lawrence Berkeley National Laboratory. The endstation was equipped with a high-resolution electron analyzer (SES-100, Gamma Data, Sweden) and a fully motorized six-axis (three translational and three rotational) goniometer.[27] The overall instrumental energy resolution, defined by the photon beam and the electron analyzer, was set better than 80 meV. The acceptance angle of the analyzer was ±4° and the angular resolution was 0.1°. The photon energy used was 90 eV. The sample temperature was kept below 100 K during all ARP measurements. We measured energy distribution curves (EDC's) of photoelectrons while the photoelectron emission angle was scanned via motorized sequential rotation (with an angular step of 0.25°) of the sample. The photoelectron intensity near E_F within an 80-meV energy window was plotted in the momentum ($k_\parallel$, as converted from the angles) space to visualize the FS's.[31] The photoelectron intensity maps were obtained only in a quadrant of the $k_\parallel$ space and mirror symmetrized across the $[11\bar{2}]$ direction. The structure models and the experimental evidence through LEED and ARP band maps assure such a mirror symmetry.

III. RESULTS

A. The Si(111)$\sqrt{7}\times\sqrt{3}$-Pb phase

Figure 3(a) is the momentum distribution map of the photoelectron intensity at Fermi energy (E_F) for the Si(111)$\sqrt{7}\times\sqrt{3}$-Pb phase. The dark features in the map correspond directly to the FS's, which exhibit a periodic pattern with various fine structures. The dominating features noticed rather easily in Fig. 3(a) are the hexagonlike features [blue lines depicted schematically in Fig. 3(b)] centered on $\bar{\Gamma}$ points of the 1×1 surface Brillouin zone (SBZ) and the rounded triangular ones (green) on $\bar{K}$. We will focus on these major features first and return back to other fine structures later.

In order to identify the two main features as possibly independent Fermi contours from different surface states, we need to trace the dispersions of the corresponding bands. Figures 3(e) and 3(f) are the energy versus momentum maps of the photoelectron intensity, along the $\bar{K}_1$-$\bar{M}_1$-$\bar{K}_2$ and $\bar{M}_1$-$\bar{\Gamma}_{01}$ SBZ lines indicated in Fig. 3(c). Here, the notations $\bar{\Gamma}$, $\bar{M}$, and $\bar{K}$ denote the symmetric points of the 1×1 SBZ. So as to establish the connection between each Fermi contour and band more clearly, photoelectron momentum distribution curves (MDC's) at E_F are plotted together.

In Fig. 3(e), one can find two strong parabolic (green) bands centered on $\bar{K}_1$ and $\bar{K}_2$, respectively. These bands produce strong photoemission intensities at E_F near $\bar{M}$ and can be traced to the triangular Fermi contours of Figs. 3(a) and 3(b). The dispersions of these bands indicate that the triangular Fermi contour around each $\bar{K}$ is an electron pocket. At $k_x\sim-1.1$ Å^{-1}, there is another metallic band (blue dashed line) crossing E_F with a very similar dispersion to that of the green band. This E_F crossing corresponds to one apex of a hexagonal feature in Figs. 3(a) and 3(b). Based on the outward dispersion from $\bar{\Gamma}$ toward both $\bar{K}$ and $\bar{M}$ [see Fig. 3(f) and below], we can identify the hexagonal features as hole pockets in contrast to the triangle features. In the MDC, there is an extra strong E_F crossing at $\bar{M}$, which will be discussed below.

On the other hand, in Fig. 3(f) we can notice a very strong photoelectron intensity at E_F on $\bar{\Gamma}_{01}$, which is due to the top of the steeply dispersing bulk band.[32–34] The bulk valence band maximum almost reaches E_F at $\bar{\Gamma}_{01}$, indicating a strong shift of the E_F position, by 0.57 eV, from the clean Si(111)7×7 surface. The edges of the Si bulk band projected onto the 1×1 SBZ, up to which the bulk band gap extends, are plotted in the figure (white lines). As clearly shown in Fig. 3(e), the determination of the position of the bulk valence band makes it obvious to assign the metallic states as surface states.

In addition to the green and blue bands, there is also conspicuous intensity at E_F with strongly dispersing bands out of the $\bar{M}_1$ point as indicated by the yellow dashed lines in Figs. 3(e) and 3(f). This feature is not related to the major Fermi contours discussed so far and we should go back to the fine structures of the FS map in Fig. 3(a). We enlarged one part of Fig. 3(a) (the boxed area) into Fig. 3(c), where the fine structures are most clearly observed. As depicted schematically in Fig. 3(d), the fine structures are mainly the X-shaped lines (yellow) and the diamond-shaped ones (black) centered on $\bar{M}_1$ although there are possibly some other features with marginal intensities. The two Fermi lines within one X feature are explained by the two dispersing bands reaching E_F both at $\bar{M}_1$ as mentioned above [yellow dashed lines in Figs. 3(e) and 3(f)]. The corresponding band for the diamond feature is not clearly observed along $\bar{K}_1$-$\bar{M}_1$-$\bar{K}_2$ but is apparent along $\bar{M}_1$-$\bar{\Gamma}_{01}$ as parabolic bands centered on $\bar{\Gamma}_{01}$ [the black dashed curves in Fig. 3(f)].

In the band map along $\bar{M}_1$-$\bar{\Gamma}_{01}$, we can identify yet another parabolic band around $\bar{M}_1$ (the white dashed curve), which has its own E_F crossing between those of yellow and black bands. This band and its Fermi-level crossing cannot be explained from the FS features discussed so far. By tracing the whole band dispersions of this white band for various directions around $\bar{\Gamma}_{01}$, we conclude that there are circular Fermi contours (hole pockets) centered on $\bar{\Gamma}_{01}$ as indicated by the gray curves in Fig. 3(d), whose presence can also be noticed in Figs. 3(a) and 3(b).

In summary, we identified the curved or arc (the hexagonal, the triangular, and the circular) and the linear (the X and the diamond) features in the complex FS map for the $\sqrt{7}\times\sqrt{3}$ surface. In the above map, it is obvious that these features have a certain periodicity, which is actually the 1×1 periodicity of Si(111). Although the diffraction pattern shows a clear $\sqrt{7}\times\sqrt{3}$ superstructure, it is hard to clearly identify spectral features following that periodicity in both FS and band dispersions.

According to a recent study[35] for a low-dimensional electronic system under competing periodic potentials, the photoemission spectral weight concentrates mostly on the unperturbed free-electron parabola. This behavior is strongly dependent on the mobility of electrons (the bandwidth) and

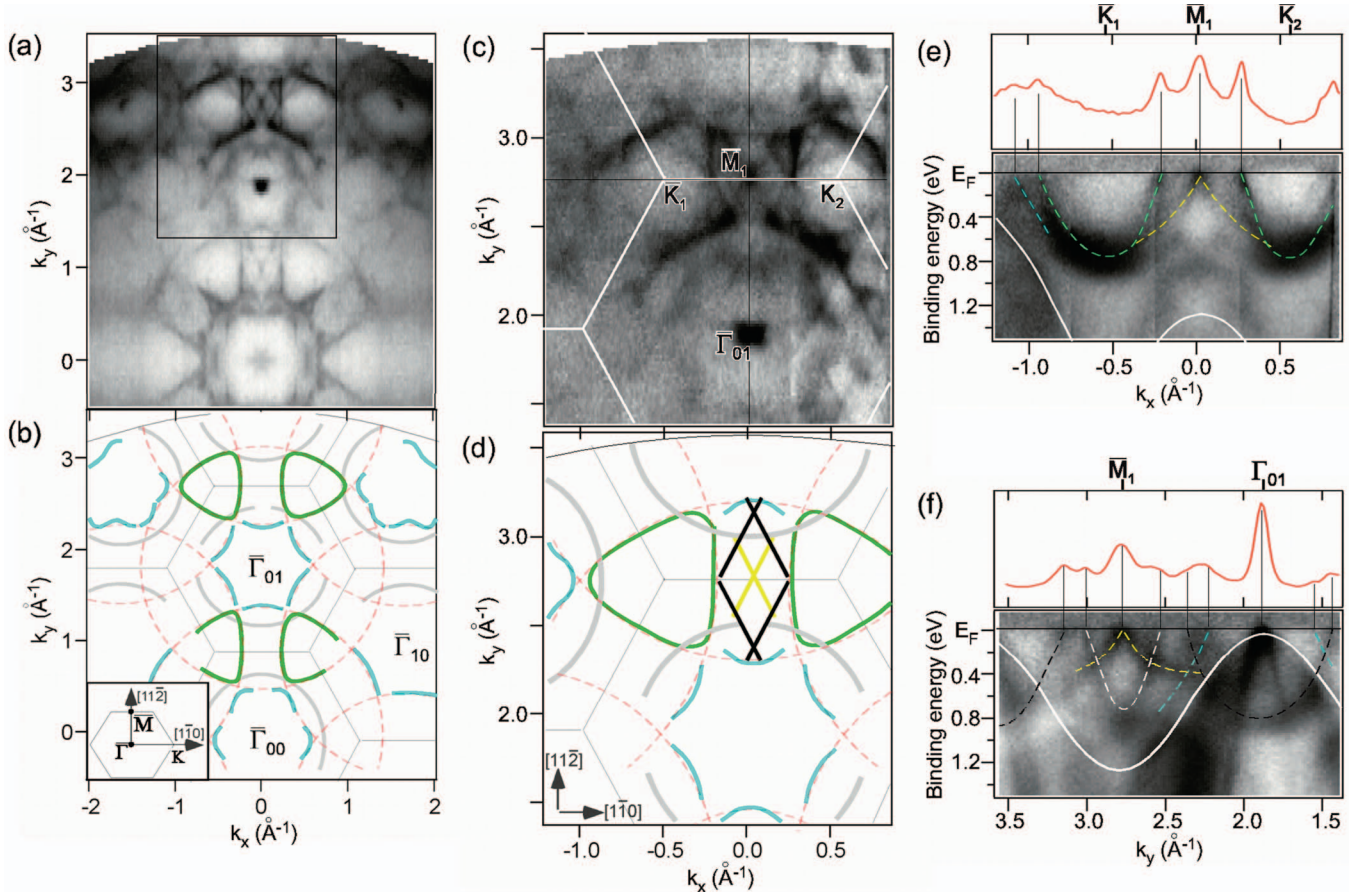

FIG. 3. (Color) Fermi contours, band dispersions, and their schematic illustrations for the Si(111)$\sqrt{7}\times\sqrt{3}$-Pb phase. (a) The photoelectron intensity map at E_F in $k_{\|}$ space taken with a photon energy of 90 eV. The intensity is given in a gray scale with higher intensity for darker contrast. That is, a dark part of this map corresponds to an E_F crossing of a metallic band. (b) The schematic illustration of the traces of dark features (the Fermi contours) in (a). The thick solid lines indicate the different Fermi contours as explained in the text. The thin solid lines depict the 1×1 SBZ, whose details are given also in the inset. The dashed circles are free-electron Fermi contours centered on each 1×1 SBZ. (c) and (d) show more details of a part of the Fermi surface map of (a) (the boxed area). The energy versus momentum maps of the photoelectron intensity (e) along the $\bar{K}_1$-$\bar{M}_1$-$\bar{K}_2$ SBZ line and (f) along $\bar{M}_1$-$\bar{\Gamma}_{01}$. The momentum distribution curves at E_F are also plotted on the top. The white solid lines indicate the upper bound of the Si bulk band.

the strength of periodic potentials: A weaker potential transfers more spectral weight to the free-electron parabola and opens a smaller gap at the corresponding zone boundary. This could be a plausible reason for the absence of an apparent $\sqrt{7}\times\sqrt{3}$ periodicity in the ARP data for the present $\sqrt{7}\times\sqrt{3}$-Pb phase. That is, it is likely that the $\sqrt{7}\times\sqrt{3}$ potential is so weak compared with that of 1×1 for the ARP spectral weight to concentrate on the trace of the free-electron parabola following the 1×1 periodicity.

Based on the apparent 1×1 periodicity and the simple assumption of a 2D free-electron model, we tried to explain the major features of the FS map. Indeed, as shown in Figs. 3(b) and 3(d), the triangular and hexagonal features are explained well by a simple array of 2D free-electron parabolas centered on $\bar{\Gamma}$ with a radius of the FS circle of 1.36 Å^{-1}. The observed band dispersions also support the existence of such FS circles; the triangles and hexagons are electron and hole pockets, respectively, with the same slope of the band dispersion [see Fig. 3(e)] as expected from the overlapping free-electron parabolas. The effective mass of this band is estimated as $1.16m_e$ (m_e is the, free-electron mass) using the radius of the FS circle (1.36 Å^{-1}) and dE/dk near E_F of 8.9 eV Å from the band dispersion. This value is indeed close to m_e. At the intersections between circles, the apexes of the triangles and the hexagons are not connected to each other, but are distorted to produce anticrossing gaps [see, for example, $(k_x,k_y)\sim(-1.0,2.7)$ Å^{-1} in Figs. 3(c) and 3(d)]. In Fig. 3(e), this gap opening is clear from the two separated bands of blue and green with almost identical dispersions. Similar triangular and hexagonal features were also observed for a Pb overlayer on Cu(111) due to the overlap of free-electron FS circles and the anticrossing behavior.[36] The anticrossing gaps of Pb/Cu(111) seem much larger than the present case making the triangles and hexagons in the FS much more isolated.

In Figs. 3(b) and 3(d), it is obvious that the other FS features of small circles (gray), X features (black), and diamonds (yellow) cannot be explained by the above free-electron band on the 1×1 lattice. In order to explain the small circular features on each $\bar{\Gamma}$, whose radius is 0.7 Å^{-1}, a

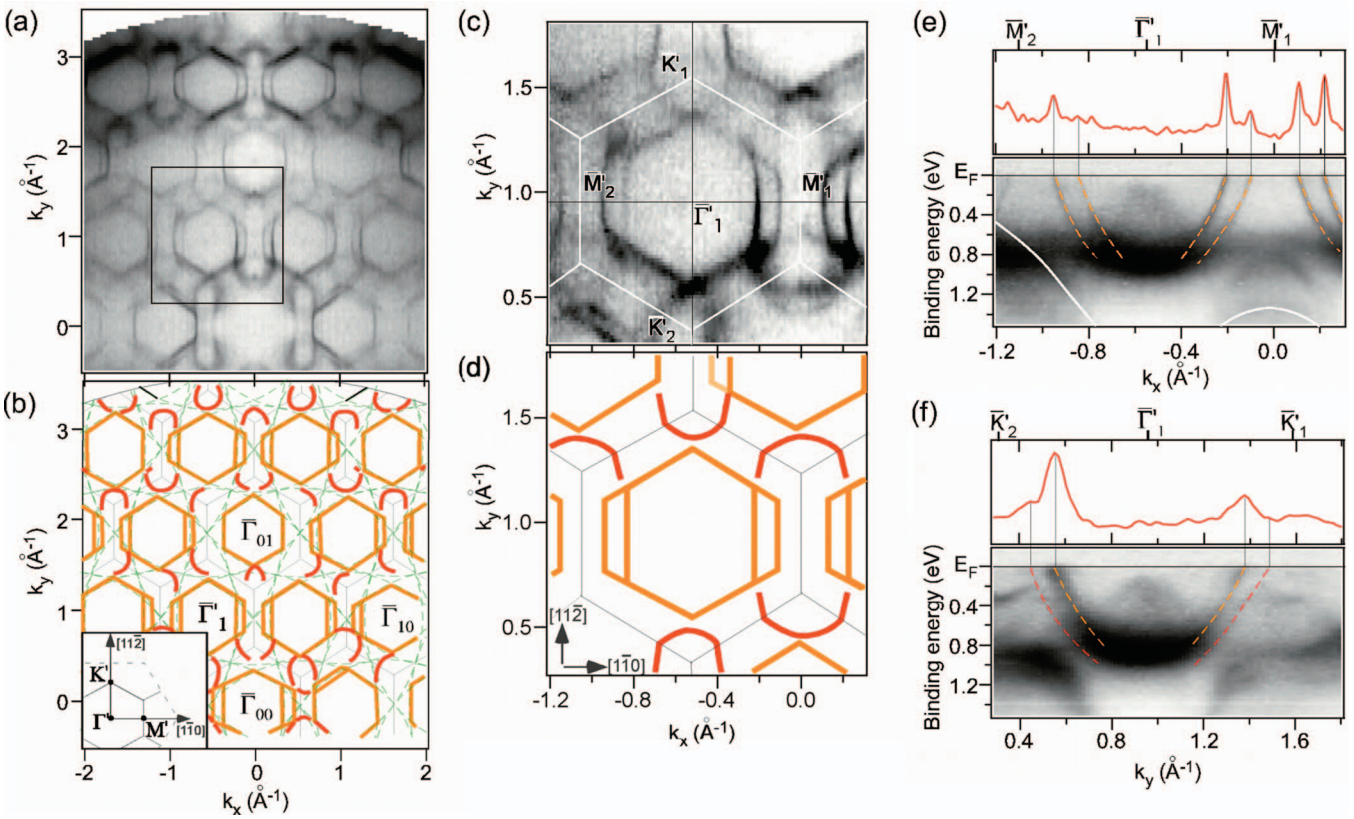

FIG. 4. (Color) (a), (b) Fermi contours, (c), (d) their schematic illustrations, and (e), (f) band dispersions for the Si(111)$14\times\sqrt{3}$-Pb phase. The format of the figures and the conditions for ARP data taking are the same as Fig. 3. The SBZ's are based on a $\sqrt{3}\times\sqrt{3}$ periodicity. The band dispersions in (e) and (f) are taken along the $\bar{M}'_2$-$\bar{\Gamma}'_1$-$\bar{M}'_1$ and $\bar{K}'_2$-$\bar{\Gamma}'_1$-$\bar{K}'_1$ SBZ lines, respectively.

2D free-*hole*-type band with a 1×1 periodicity is required. We thus tried to explain the fine structures of X and diamond shapes through the $\sqrt{7}\times\sqrt{3}$ umklapp process of the 2D free-electron (or the small hole) circles; that is, through repeating the free-electron (-hole) circles with a $\sqrt{7}\times\sqrt{3}$ periodicity. This simulation was unsuccessful partly because the triple-domain $\sqrt{7}\times\sqrt{3}$ periodicity is much too complicated. These linear fine structures may have a different origin from the 2D free-electron-like band. At the same time, we cannot completely exclude the possibility of a mixed phase, which was not detected in LEED, as the origin of these extra FS features.

Recently the electronic band structure of the Si(111)$\sqrt{7}\times\sqrt{3}$-In surface was characterized in detail and understood based on the 2D free-electron-like band.[27] However, in spite of the same $\sqrt{7}\times\sqrt{3}$ periodicity, the similar adsorbate density, and the similar free-electron-like nature, the FS of $\sqrt{7}\times\sqrt{3}$-Pb has contrasting characteristics from that of $\sqrt{7}\times\sqrt{3}$-In. The FS of $\sqrt{7}\times\sqrt{3}$-In with 1.2 ML of In follows essentially the 1×1 square lattice of an undistorted In layer [proximal to In(100)1×1] in clear contrast to the present case following the 1×1 hexagonal lattice of Si(111). This interesting difference suggests that the substrate-adsorbate interaction is much stronger in $\sqrt{7}\times\sqrt{3}$-Pb than in $\sqrt{7}\times\sqrt{3}$-In. A further comparison of these two phases should consider the detailed atomic structures and bonding natures, which are not clear for both phases at present.

B. The Si(111)$14\times\sqrt{3}$-Pb phase

While the $\sqrt{7}\times\sqrt{3}$ phase is one building block phase of the devil's-staircase phase diagram, the dense $\sqrt{3}\times\sqrt{3}$ phase at 1.33 ML is the other building block.[16] However, we could not get the dense $\sqrt{3}\times\sqrt{3}$ phase reproducibly and, as mentioned above, the $14\times\sqrt{3}$ phase was the highest-coverage phase obtained reproducibly. According to the devil's-staircase structure model,[16] this phase is composed of six dense $\sqrt{3}\times\sqrt{3}$ unit cells separated by two $\sqrt{7}\times\sqrt{3}$ units which behave as a linear domain wall to relieve the compressive strain of the dense $\sqrt{3}\times\sqrt{3}$ structure. The Pb coverage for this phase, which has also been called the "striped incommensurate phase," is 1.28 ML.

Figure 4 shows the FS and band mapping data for this high-coverage phase in the same scheme as Fig. 3. Figures 4(a) and 4(c) are the momentum distribution map of the photoelectron intensity at E_F (i.e., the FS map), an overview and the enlarged details, respectively, whose schematics are shown in Figs. 4(b) and 4(d), respectively. The white hexagons in Fig. 4(c) indicate the $\sqrt{3}\times\sqrt{3}$ SBZ boundaries. In addition, in Figs. 4(e) and 4(f), the band maps are shown along $\bar{M}'_2$-$\bar{\Gamma}'_1$-$\bar{M}'_1$ and $\bar{K}'_2$-$\bar{\Gamma}'_1$-$\bar{K}'_1$ SBZ lines together with the momentum distribution curves at E_F. The notations $\bar{\Gamma}'$, $\bar{M}'$, and $\bar{K}'$ denote the symmetric points of a $\sqrt{3}\times\sqrt{3}$ SBZ. In the case of $14\times\sqrt{3}$, the bulk valence band maximum is shifted by 70 meV toward higher binding energy from that of $\sqrt{7}$

$\times\sqrt{3}$, as measured by identifying the prominent bulk band dispersion (data not shown here). This corresponds to a shift of 0.50 eV toward E_F from the Si(111)7×7 clean surface.

The most apparent and characteristic features in the FS map are the hexagons, which are depicted schematically by orange lines in Figs. 4(b) and 4(d). These hexagons follow the $\sqrt{3}\times\sqrt{3}$ periodicity as centered on each $\bar{\Gamma}'$ (the center of the 1×1 SBZ $\bar{\Gamma}$ overlaps with $\bar{\Gamma}'$). The other features are the semicircular ones connecting neighboring hexagons as depicted by red arcs in Figs. 4(b) and 4(d). In the detailed FS map of Figs. 4(c) and 4(d), we can clearly see that the hexagons split or repeat along the $\bar{\Gamma}_1'$-$\bar{M}_1'$ SBZ line (the $[1\bar{1}0]$ direction). This splitting matches the characteristic splitting of LEED spots due to the $\times14$ periodicity. Indeed, the spacing between the split hexagons coincides exactly with the reciprocal lattice vector of the $\times14$ periodicity. Note that, since we prepared a single-domain $14\times\sqrt{3}$ surface, the hexagonal replicas are observed only along the $[1\bar{1}0]$ direction.

Figures 4(e) and 4(f) show clearly the underlying bands for the hexagonal Fermi contours. The corresponding bands disperse parabolically. The hexagons are thus electron pockets. The consistent dispersions of these bands confirm that they have the same origin. The band for the semicircle FS feature is resolved along $\bar{K}_2'$-$\bar{\Gamma}_1'$-$\bar{K}_1'$ in Fig. 4(f) (red dashed curves) and its dispersion is quite similar to that of the adjacent band for the hexagonal feature.

Note that the overall periodicity of FS features and the underlying band dispersion are governed by a $\sqrt{3}\times\sqrt{3}$ periodicity in clear contrast with the 1×1 periodicity of the $\sqrt{7}\times\sqrt{3}$ phase. It must be related to the fact that the corresponding LEED pattern is also basically a $\sqrt{3}\times\sqrt{3}$ one modulated by the $\times14$ periodicity along $[1\bar{1}0]$. The splittings or replica bands are thought to be due to the final state effect (the umklapp scattering), because no anticrossing gap is noticed in either FS or band dispersion, which would represent the effect of an initial state potential. The results qualitatively indicate that the surface has a strong $\sqrt{3}\times\sqrt{3}$ potential and a very weak $14\times\sqrt{3}$ one. This can rather straightforwardly be understood from the devil's-staircase structure model, which consists essentially of local $\sqrt{3}\times\sqrt{3}$ units (or domains) and the $\times14$-period domain walls. This also leads to a reasonable guess that the FS of the ideal dense $\sqrt{3}\times\sqrt{3}$ phase consists of hexagons without splittings or replicas.

Based on the dominating $\sqrt{3}\times\sqrt{3}$ periodicity and the 2D nearly-free-electron scheme, we can construct the major FS features, especially the hexagons. As shown in Fig. 4(b), all the edges of hexagons are located on the free-electron FS circles (dashed circles) with a radius of 1.44 Å^{-1} on every $\sqrt{3}\times\sqrt{3}$ SBZ. This FS circle is also very similar to that of the $\sqrt{7}\times\sqrt{3}$ phase, only 6% larger. The effective mass of the band was estimated to be $1.27m_e$, similar to that of $\sqrt{7}\times\sqrt{3}$. This similarity suggests that the origin of the major surface electronic states is the same for these two phases although the apparent FS shapes are significantly different. This point will be discussed further below. The semicirclelike FS features (red curves in Fig. 4) also roughly follow the the traces of those free-electron FS circles. The relatively large deviation from circles may be understood from a strong anticrossing gap opening at the intersection between the free-electron Fermi circles due to a strong $\sqrt{3}\times\sqrt{3}$ potential. The dispersion of the red bands shown in Fig. 4(f) is also consistent with this interpretation.

IV. DISCUSSION

The most important characteristic in the electronic structures of the dense Pb overlayers revealed in the present study is their nearly free-electron-like Fermi surfaces. The circular Fermi contours of a 2D free-electron model could reproduce the main FS features in both phases. The underlying band structures also confirm the existence of 2D parabolas, which constitute big electron pockets centered on $\bar{\Gamma}$ or $\bar{\Gamma}'$. Moreover, we obtained similar effective masses for the major free-electron-like bands of $\sqrt{7}\times\sqrt{3}$ and $14\times\sqrt{3}$ phases, which implies that the corresponding bands have the same origin. The filling of this band represented by the radius of the free-electron Fermi circle may depend on the density of the Pb overlayers, that is, the surface electron density. The radius of the Fermi circle for the $14\times\sqrt{3}$ phase is 1.44 Å^{-1}, larger than 1.36 Å^{-1} for $\sqrt{7}\times\sqrt{3}$. We also measured the FS's from several, rather ill-defined, phases with intermediate Pb coverages between the $\sqrt{7}\times\sqrt{3}$ and $14\times\sqrt{3}$ phases. We could confirm a tendency that the Fermi circles are preserved while their radius increases gradually as we increase the Pb coverage (data not shown here).

If we quantitatively compare the area surrounded by the primary FS circle with that of a 1×1 SBZ, then we can obtain the number of electrons related to this 2D free-electron-like band per 1×1 unit cell. In the case of $\sqrt{7}\times\sqrt{3}$, the area ratio is 1.9, which means that 3.8 electrons contribute to the free-electron-like metallic band. In the same way, the larger FS circle in $14\times\sqrt{3}$ is estimated to represent 4.2 metallic electrons. The difference of 0.4 electrons per 1×1 unit cell means a Pb-coverage difference of 0.1 ML since a Pb adatom has four valence electrons. This estimation is consistent with the Pb coverages of $\sqrt{7}\times\sqrt{3}$ and $14\times\sqrt{3}$ phases within the devil's-staircase models, 1.20 and 1.28 ML, respectively. The numbers of valence electrons per 1×1 unit cell, which contains four electrons per Pb adatom and one electron from the dangling bond of a Si atom in the second layer, are simply calculated as 5.8 and 6.2 for $\sqrt{7}\times\sqrt{3}$ and $14\times\sqrt{3}$, respectively. If we assume a simple covalent bond between Pb and Si, which does not contribute to the 2D metallic state, the numbers of in-plane electrons within the two Pb overlayers are 3.8 and 4.2, respectively. These values are exactly what are measured from the size of the FS circles in the ARP measurements. A more realistic electron counting can in principle be done by integrating the total area of the occupied FS's, which must consider the details of the structural and electronic configurations. This is not realistic due to the unresolved fine structures of the FS's and the lack of information on the detailed atomic and electronic structures.

The above discussion supports the 2D nearly-free-electron picture for the electronic band structures of the dense Pb overlayers and the devil's-staircase structure models. How-

ever, there is further complication, especially for the $\sqrt{7}\times\sqrt{3}$ phase. First, the FS and band dispersions have fine structures and extra holelike Fermi circles, which cannot be explained by a single free-electron Fermi circle and the apparent 1×1 periodicity. Second, as briefly mentioned above, there are two conflicting structure models for $\sqrt{7}\times\sqrt{3}$-Pb with 1.2 (Ref. 21) and 1.0 (Ref. 19) ML coverages, respectively. The 1.2-ML model extends successfully to explain the whole devil's-staircase phase diagram.[16] Note, however, that the devil's-staircase mechanism may not heavily depend on the detailed atomic structures of the two building block structures involved. On the other hand, the 1-ML model, the so-called trimer model, is favorable to explain the phase transition into the 1×1 phase; the $\sqrt{7}\times\sqrt{3}$ phase is stable only below 230 K and transforms into a 1×1 phase above 230 K.[22] Further investigation is required to determine the atomic structures of the $\sqrt{7}\times\sqrt{3}$ and 1×1 phase before one discusses the origin of the complicated FS fine structure.

What is also important for the above 2D nearly-free-electron picture is that the apparent FS shapes can change drastically due to the given superperiodicity although the underlying free-electron band is the same. This is clear in the distinct FS shapes of $\sqrt{7}\times\sqrt{3}$ and $14\times\sqrt{3}$ phases. It should be noted that the periodicity is not consistent with the apparent structural periodicity shown in LEED and scanning tunneling microscopy (STM); while the basic periodicity in the $\sqrt{7}\times\sqrt{3}$ structure follows the 1×1 reciprocal lattice, that in the $14\times\sqrt{3}$ is based on the $\sqrt{3}\times\sqrt{3}$. As mentioned above, this may roughly indicate that there are competing periodic potentials, such as 1×1 and $\sqrt{7}\times\sqrt{3}$ for the $\sqrt{7}\times\sqrt{3}$ phase and $\sqrt{3}\times\sqrt{3}$ and $14\times\sqrt{3}$ in the $14\times\sqrt{3}$ phase, and the strength of the potentials experienced by the electrons near E_F is greatly different. Such a difference in the potential strength would lead to a strong redistribution of the spectral weight in ARP, which would make the apparent periodicities in FS's and LEED patterns different.[35] As discussed above, the strong $\sqrt{3}\times\sqrt{3}$ potential for the $14\times\sqrt{3}$ phase can be explained by the fact that this phase consists mainly of local $\sqrt{3}\times\sqrt{3}$ structures separated by $\times14$ domain walls. Although the structure model for the $\sqrt{7}\times\sqrt{3}$ phase is under debate, the present ARP result indicates that this phase has a strong 1×1 structure with a very weak $\sqrt{7}\times\sqrt{3}$ modulation. This may also be related to the $\sqrt{7}\times\sqrt{3}$–1×1 phase transition.

Finally, we comment on the pinning of Fermi levels. The E_F position of the $14\times\sqrt{3}$ phase is 130 meV above the bulk valence band maximum, while this value is reduced to 60 meV in the case of the $\sqrt{7}\times\sqrt{3}$ phase. These results correspond to extraordinarily high Schottky-barrier heights (SBH's) of 0.99 and 1.06 eV, respectively, which are consistent with the early result for the similar, but not so well-characterized, phase of β-$\sqrt{3}\times\sqrt{3}$ (at about 1.3 ML).[25] These SBH values were previously explained by the E_F pinning due to a partially filled *localized* surface state,[6] due to the surplus of Pb adatoms over the one-to-one 1×1 registry with the substrate. However, in the present study, we clearly showed that the Fermi-level pinning is caused by a highly dispersing 2D free-electron-like metallic band. In this case, the electron filling or the electron density of the 2D nearly-free-electron system would determine the Fermi-level position, which will be governed primarily by the density of overlayer atoms.

V. CONCLUSION

The electronic structures of two well-ordered dense Pb overlayers on the Si(111) surface, the $\sqrt{7}\times\sqrt{3}$ and $14\times\sqrt{3}$ phases, have been studied using angle-resolved photoemission based on undulator synchrotron radiation. These two phases roughly correspond to the two basic building-block structures of a complex series of overlayer phases in the recently found devil's-staircase phase diagram. The full Fermi surfaces and the underlying band dispersions of metallic surface states within the band gap of the Si substrate were mapped out for the whole surface Brillouin zones of both phases. The FS of the $\sqrt{7}\times\sqrt{3}$ phase is composed of hexagonal, triangular, and circular features with fine structures of X- and diamond-shaped ones. The hexagonal and triangular features were shown to originate from the same 2D free-electron band following a 1×1 periodicity. The circular feature is a hole pocket centered on each 1×1 SBZ. The other fine structures cannot simply be understood from the above 2D bands even though the full $\sqrt{7}\times\sqrt{3}$ periodicity is considered. For the case of $14\times\sqrt{3}$, the FS consists of hexagonal and semicircular features following a $\sqrt{3}\times\sqrt{3}$ periodicity. These features are successfully explained by a single 2D free-electron band within a $\sqrt{3}\times\sqrt{3}$ potential. Extra fine structure is also observed, which can be understood as the umklapp bands for the $\times14$ periodicity.

These results disclose that the metallic electrons of the dense Pb overlayers are mainly governed by a single 2D free-electron band as modulated by surface superstructure potentials. The filling of that 2D free-electron band was consistent with the number of in-plane valence electrons of the Pb overlayers. It is also found that the surface superstructure potentials reflected in the electronic band structures are not the same as the apparent surface superstructure shown in LEED or STM. This phenomenon is understood by the existence of competing periodicities with greatly different potential strengths for the electrons near E_F. This explanation is consistent with the recent structure model of the $14\times\sqrt{3}$ phase and provides some insight into the structure of the $\sqrt{7}\times\sqrt{3}$ phase under debate. While the fine details of the FS's and band dispersions, especially of the $\sqrt{7}\times\sqrt{3}$ phase, need to be investigated further based on well-established structural models, the present results suggest that the complex surface band structures of dense metal overlayers are governed by simple 2D free-electron character, and FS mapping by ARP can probe the dominating surface potentials, which are not obvious in structural probes.

ACKNOWLEDGMENTS

This work was supported through the Center for Atomic Wires and Layers of the CRi program by MOST of Korea. The ALS is operated under Department of Energy Contract No. DE-AC03-76SF00098 at Lawrence Berkeley National Laboratory. H.K. is grateful for the financial support from CSCMR supported by KOSEF.

*Author to whom correspondence should be addressed. Electronic address: yeom@yonsei.ac.kr

[1] G. Le Lay, M. Abraham, A. Kahn, K. Hricovini, and J. E. Bonnet, Phys. Scr., T **35**, 261 (1991).
[2] D. R. Heslinga, H. H. Weitering, D. P. van der Werf, T. M. Klapwijk, and T. Hibma, Phys. Rev. Lett. **64**, 1589 (1990).
[3] S. Hasegawa, X. Tong, S. Takeda, N. Sato, and T. Nagao, Prog. Surf. Sci. **60**, 89 (1999).
[4] Y. Miura, S. Fujieda, and K. Hirose, Phys. Rev. B **50**, 4893 (1994).
[5] Raymond T. Tung, Phys. Rev. Lett. **84**, 6078 (2000).
[6] H. H. Weitering, A. R. H. F. Ettema, and T. Hibma, Phys. Rev. B **45**, 9126 (1992).
[7] K. Budde, E. Abram, V. Yeh, and M. C. Tringides, Phys. Rev. B **61**, R10602 (2000).
[8] M. Hupalo, V. Yeh, L. Berbil-Bautista, S. Kremmer, E. Abram, and M. C. Tringides, Phys. Rev. B **64**, 155307 (2001).
[9] M. Hupalo and M. C. Tringides, Phys. Rev. B **65**, 115406 (2002).
[10] Z. Zhang, Q. Niu, and C.-K. Shih, Phys. Rev. Lett. **80**, 5381 (1998).
[11] V. Yeh, L. Berbil-Bautista, C. Z. Wang, K. M. Ho, and M. C. Tringides, Phys. Rev. Lett. **85**, 5158 (2000).
[12] S. H. Chang, W. B. Su, W. B. Jian, C. S. Chang, L. J. Chen, and T. T. Tsong, Phys. Rev. B **65**, 245401 (2002).
[13] Y. Guo, Y.-F. Zhang, X.-Y. Bao, T.-Z. Han, Z. Tang, L.-X. Zhang, W.-G. Zhu, E. G. Wang, Q. Niu, Z. Q. Qiu, J.-F. Jia, Z.-X. Zhao, and Q.-K. Xue, Science **306**, 1915 (2004).
[14] P. Czoschke, H. Hong, L. Basile, and T.-C. Chiang, Phys. Rev. Lett. **93**, 036103 (2004).
[15] D. A. Ricci, T. Miller, and T.-C. Chiang, Phys. Rev. Lett. **95**, 266101 (2005).
[16] M. Hupalo, J. Schmalian, and M. C. Tringides, Phys. Rev. Lett. **90**, 216106 (2003).
[17] E. Ganz, I.-S. Hwang, F. Xiong, Silva K. Theiss, and J. Golovchenko, Surf. Sci. **257**, 259 (1991).
[18] J. Slezák, P. Mutombo, and V. Cháb, Phys. Rev. B **60**, 13 328 (1999).
[19] I.-S. Hwang, S.-H. Chang, C.-K. Fang, L.-J. Chen, and T. T. Tsong, Phys. Rev. Lett. **93**, 106101 (2004).
[20] O. Custance, I. Brihuega, J.-Y. Veuillen, J. M. Gómez-Rodríguez, and A. M. Baró, Surf. Sci. **482–485**, 878 (2001).
[21] T.-L. Chan, C. Z. Wang, M. Hupalo, M. C. Tringides, Z.-Y. Lu, and K. M. Ho, Phys. Rev. B **68**, 045410 (2003).
[22] K. Horikoshi, X. Tong, T. Nagao, and S. Hasegawa, Phys. Rev. B **60**, 13287 (1999).
[23] L. Seehofer, G. Falkenberg, D. Daboul, and R. L. Johnson, Phys. Rev. B **51**, 13503 (1995).
[24] P. Bak, Rep. Prog. Phys. **45**, 587 (1982).
[25] X. Tong, K. Horikoshi, and S. Hasegawa, Phys. Rev. B **60**, 5653 (1999).
[26] M. Hupalo, S. Kremmer, V. Yeh, L. Berbil-Bautista, E. Abram, and M. C. Tringides, Surf. Sci. **493**, 526 (2001).
[27] E. Rotenberg, H. Koh, K. Rossnagel, H. W. Yeom, J. Schäfer, B. Krenzer, M. P. Rocha, and S. D. Kevan, Phys. Rev. Lett. **91**, 246404 (2003).
[28] In the phase diagram (Ref. 16) the highest-coverage phase is dense $\sqrt{3}\times\sqrt{3}$. However, the stability of each phase is greatly different, which often leads to a mixture of phases after annealing. In our own case, the $14\times\sqrt{3}$ phase was the highest-coverage phase that could be obtained stably and reproducibly without any phase mixture in LEED. The stability difference for phases is one characteristic feature of the devil's-staircase model (Ref. 24).
[29] J. Viernow, J.-L. Lin, D. Y. Petrovykh, F. M. Leibsle, F. K. Men, and F. J. Himpsel, Appl. Phys. Lett. **72**, 948 (1998).
[30] A. Petkova, J. Wollschläger, H.-L. Günter, and M. Henzler, Surf. Sci. **471**, 11 (2001).
[31] P. Aebi, R. Fasel, D. Naumović, J. Hayoz, Th. Pillo, M. Bovet, R. G. Agostino, L. Patthey, L. Schlapbach, F. P. Gil, H. Berger, T. J. Kreutz, and J. Osterwalder, Surf. Sci. **402–404**, 614 (1998).
[32] R. I. G. Uhrberg and G. V. Hansson, CRC Crit. Rev. Solid State Mater. Sci. **17**, 133 (1991).
[33] Y. He, S. Bouzidi, B. Y. Han, L.-M. Yu, P. A. Thiry, R. Caudano, and J.-M. Debever, Phys. Rev. B **54**, 17654 (1996).
[34] L. Aballe, C. Rogero, P. Kratzer, S. Gokhale, and K. Horn, Phys. Rev. Lett. **87**, 156801 (2001).
[35] J. Voit, L. Perfetti, F. Zwick, H. Berger, G. Magaritondo, G. Grüner, H. Höchst, and M. Grioni, Science **290**, 501 (2000).
[36] F. Baumberger, W. Auwärter, T. Greber, and J. Osterwalder, Science **306**, 2221 (2004).